J. Fluid Mech. (1989), *vol.* 200, *pp.* 283–307
Printed in Great Britain

Area-varying waves on curved vortex tubes with application to vortex breakdown

By T. S. LUNDGREN† AND W. T. ASHURST‡

†Department of Aerospace Engineering and Mechanics, University of Minnesota, Minneapolis, MN 55455, USA

‡Combustion Research Facility, Sandia National Laboratories, Livermore, CA 94550, USA

(Received 19 March 1986 and in revised form 10 August 1988)

Equations which modify those derived by Widnall & Bliss (1971) and Moore & Saffman (1972) are presented in which jet-like flow along the axis of a vortex tube interacts with the motion of the tube. The equations describe two major effects. The first is the propagation of axial waves along the vortex tube which is similar to the flow of shallow water. A local decrease in cross-section area of the vortex tube produces higher swirling velocity and lower pressure. The resulting axial pressure gradient causes a propagating wave of area and axial velocity in order to move fluid into the region of smaller area. The second effect is instability to helical disturbances when the jet-like axial velocity is high enough to overcome the stabilizing effect of the swirling motion. An elementary nonlinear theory of vortex breakdown is presented which has an analogy with the formation of bores in shallow-water theory. A numerical example shows the growth of a helical disturbance behind a vortex breakdown front.

1. Introduction

The velocity field induced by tubes of concentrated vorticity in an otherwise irrotational fluid may be calculated from the Biot–Savart integral (Leonard 1985) of the complete vorticity field. This velocity field may be used to convect the vortex tube according to the general laws of inviscid fluid mechanics. The thin filament approximation treats the vortex tube as a space curve, but to calculate the velocity at a point on this curve the structure of the vortex core must be accounted for in order to avoid divergence of the integral. One method of doing this is to modify the integrand near the singular point. A method proposed by Rosenhead (1930) leads to a modified Biot–Savart law for the velocity $\boldsymbol{V}_{\mathrm{B}}(s,t)$ at a point $\boldsymbol{r}(s,t)$ on the filament

$$\boldsymbol{V}_{\mathrm{B}}(s,t) = -\frac{\Gamma}{4\pi}\int \frac{\{\boldsymbol{r}(s,t)-\boldsymbol{r}(s',t)\}\times \partial \boldsymbol{r}(s',t)/\partial s'\,\mathrm{d}s'}{\{|\boldsymbol{r}(s,t)-\boldsymbol{r}(s',t)|^2+\mu^2\}^{\frac{3}{2}}}, \tag{1.1}$$

where Γ is the circulation around the filament and s is the arc length along the space curve. In this work we will select the direction of integration to be in the direction of the vorticity, then the circulation will always be positive. Moore (1972) showed that the correct velocity for a vortex ring results if μ is proportional to the local core radius σ with a coefficient that depends on the vorticity distribution in the core. For a hollow vortex $\mu = \exp(-\frac{1}{4})\sigma$ while for uniform vorticity $\mu = \exp(-\frac{3}{4})\sigma$. Several methods have been used to determine the variable core radius σ. One method

determines the local core radius from the local stretching. That is, if ξ is the initial arc length along the vortex (a Lagrangian variable) then

$$\lambda = \frac{\mathrm{d}s}{\mathrm{d}\xi} = \left|\frac{\partial \boldsymbol{r}}{\partial \xi}\right| \tag{1.2}$$

is the local stretch ratio. Conservation of mass relates σ to λ by

$$\lambda\sigma^2 = \sigma_0^2 \tag{1.3}$$

where σ_0 is the initial core radius (assumed constant). There is an approximation here because the dynamical effects of the spatial variation of core radius are neglected. Another method for defining the core radius follows from a suggestion by Moore & Saffman (1972; hereinafter referred to as MS), that axial waves would quickly smooth out any variations in σ. In this approximation σ is taken to be a function of time alone, chosen so that the total volume of the core is constant.

In the present paper, modifications of the dynamical equations proposed by Widnall & Bliss (1971; hereinafter referred to as WB) and MS are presented. These modified equations permit axial waves of area and velocity in the vortex tube and allow the local core radius to be determined dynamically. One consequence of axial flow in a curved vortex tube is the possibility of unbalanced centrifugal forces which can affect the overall motion of the vortex through the 'fire hose' instability.

In §2 the basic equations are presented. In §3 these are cast in the form of intrinsic equations which describe the motion of the vortex tube in terms of the local torsion, curvature and area without regard for the position of the tube in space. These equations are applied to the motion of vortex rings and helices. In §4 the equations are specialized to one-dimensional flow where wave phenomena similar to shallow water waves, and described by the same equations, are found. A particular result is a nonlinear theory of strong vortex breakdown which is analogous to Rayleigh's theory of bores. In §5 the complete three-dimensional equations are integrated numerically, showing the growth of helical disturbances on a vortex with an area varying wave.

2. Vortex dynamics with core variation and cross-flow Kutta–Joukowsky lift

The vortex tube will be modelled by a centreline space curve along which a mass $\rho A(s,t)$ per unit length and a velocity $V(s,t)$ are prescribed, where $A(=\pi\sigma^2)$ is the local cross-sectional area and V is defined as the average velocity over a cross-section. This average velocity can include a jet-like component along the axial direction of the vortex. The shape and motion of the centreline are described by $\boldsymbol{r} = \boldsymbol{r}(\xi,t)$ where ξ is a material variable defined such that $\partial \boldsymbol{r}(\xi,t)/\partial t = \boldsymbol{V}$. A point with fixed ξ moves with the velocity $\boldsymbol{V}$ (the derivative $\partial/\partial t$ taken with ξ fixed is a material derivative). Arc length s along the curve is related to ξ by (1.2) and the local tangent vector is given by

$$\hat{\boldsymbol{t}} = \frac{\partial \boldsymbol{r}}{\partial s} = \frac{\partial \boldsymbol{r}}{\lambda\,\partial \xi}. \tag{2.1}$$

The local vorticity is in the direction of $\hat{\boldsymbol{t}}$. Conservation of mass expressed by $\partial(A\,\mathrm{d}s)/\partial t = 0$, is equivalent to (1.3) because of the definition of λ. The rate of change of momentum of the fluid in a control volume in the vortex with ends consisting of

disks at ξ and $\xi+\mathrm{d}\xi$ which are perpendicular to the centreline of the vortex and moving with it is

$$\rho A\,\mathrm{d}s\,\partial V/\partial t+\int_{\xi+\mathrm{d}\xi}\rho v(\boldsymbol{v}-\boldsymbol{V}_\mathrm{d})\cdot\hat{\boldsymbol{t}}\,\mathrm{d}A-\int_{\xi}\rho\boldsymbol{v}(\boldsymbol{v}-\boldsymbol{V}_\mathrm{d})\cdot\boldsymbol{t}\,\mathrm{d}A, \tag{2.2}$$

where $\boldsymbol{v}$ is the local velocity in the vortex tube and $\boldsymbol{V}_\mathrm{d}$ is the velocity of the disk surface. The integrals are the net momentum flux into the control volume through the disk surfaces. A non-zero momentum flux can be caused by the non-uniformity of the axial components of $\boldsymbol{v}$ or $\boldsymbol{V}_\mathrm{d}$. The latter results from rigid rotation of the control surface disk about a diameter along the binormal to the centreline curve. The integral term would be exactly zero if the axial velocity were a slightly non-uniform slug flow with $\boldsymbol{v}\cdot\hat{\boldsymbol{t}}=\boldsymbol{V}_\mathrm{d}\cdot\hat{\boldsymbol{t}}$. As a statement of ignorance these momentum integrals will be neglected. Indeed, it is difficult to make any simple, but realistic, axial velocity assumption because of viscous and gyroscopic effects. The momentum integral terms are the only terms in the resulting equation which are strongly dependent on the axial velocity profile, and to the extent that these terms are negligible the results will be profile independent.

An element of the vortex is pictured as a rotating slug of fluid sliding along a twisted tube which has transverse motion relative to the fluid outside the tube. (For a 'hollow' vortex the slug slides without rotating.) The local velocity outside the vortex tube consists of a swirling flow plus a more or less uniformly approaching cross-flow which streams around the vortex tube. This cross-flow is approximated by the Biot–Savart velocity $\boldsymbol{V}_\mathrm{B}$ (evaluated at the centreline of the tube). MS have shown indirectly that this is a correct interpretation if the curvature of the tube is small.

The equation of motion of an element of the vortex is obtained by equating the rate of change of momentum of an element to the pressure forces which act on it. This results in the equation

$$\rho A\frac{\partial\boldsymbol{V}}{\partial t}=-\rho A\left(\frac{\partial\boldsymbol{u}_\mathrm{T}}{\partial t}-\boldsymbol{u}\cdot\hat{\boldsymbol{t}}\frac{\partial\boldsymbol{u}_\mathrm{T}}{\partial s}\right)+\rho\Gamma\hat{\boldsymbol{t}}\times\boldsymbol{u}-\left(\frac{\rho\Gamma^2}{8\pi A}\right)\frac{\partial A}{\partial s}\hat{\boldsymbol{t}}-A\nabla P_\mathrm{B}, \tag{2.3}$$

where $\boldsymbol{u}=\boldsymbol{V}-\boldsymbol{V}_\mathrm{B}$ is the velocity of the vortex relative to the surrounding fluid, and $\boldsymbol{u}_\mathrm{T}=\boldsymbol{u}-\hat{\boldsymbol{t}}\hat{\boldsymbol{t}}\cdot\boldsymbol{u}$ is its transverse part. Each of these terms will be discussed. The first term on the right-hand side of (2.3) is an added mass force caused by modification of the surface pressure by transverse acceleration of the vortex relative to the surrounding fluid as if it were a solid cylinder. The material derivative $(\partial/\partial t)$ gives the relative acceleration seen by an observer moving and sliding along the tube with the vortex material. The particular combination of terms used here gives, approximately, the transverse acceleration seen by an observer who is moving with the vortex but not sliding along it. An added mass term similar to this was used by WB.

The second term is the Kutta–Joukowsky lift which results from cross-flow over the vortex. This was first used by WB. MS did a careful analysis showing that this term is correct when the curvature is small, the error being of order $\rho\Gamma^2A/\rho_\mathrm{c}^3$ where ρ_c is the local radius of curvature. An additional term which MS call 'tension' is included here in the Kutta–Joukowsky lift.

The third term, due to MS, is an axial force caused by the swirl induced pressure acting on an axial area variation. An elementary derivation is given here. In a coordinate system carried along with the vortex tube the pressure outside the vortex is approximately determined by

$$\frac{\partial p}{\partial r}=\frac{\rho v_\theta^2}{r} \tag{2.4}$$

with $$v_\theta = \Gamma/2\pi r. \tag{2.5}$$

Integrating this from infinity gives the pressure on the vortex tube:

$$p(\sigma) = -\rho\Gamma^2/8\pi A. \tag{2.6}$$

The axial force per unit length on the vortex surface is $p(\sigma)\,\partial A/\partial s$. This is the third term above. In addition to this force there is another term from the pressure difference across the ends of the vortex element. This was obtained by MS by integrating (2.4) inside the vortex with an assumed swirl profile. The resulting force is equivalent to using a swirl dependent 'cut-off' in $\boldsymbol{V}_{\mathrm{B}}$ and has already been included in the Kutta–Joukowsky lift term (in the swirl dependence of μ). The equivalence of the 'cut-off' form and the Rosenhead form of $\boldsymbol{V}_{\mathrm{B}}$ has been discussed by Moore (1972).

The above procedure for calculating the axial force strongly resembles the method for approximating the pressure force in the shallow-water equations. There the vertical pressure gradient in a horizontal layer of fluid is determined in the 'hydrostatic' approximation, neglecting vertical acceleration. Here centrifugal forces replace gravity, and radial acceleration is neglected. This suggests that an improvement could be obtained by approximating the radial acceleration. This would give an additional 'dispersion' term as in the corresponding shallow-water equations.

The last term in (2.3) is also from MS. It represents a non-dynamical 'buoyancy' force on the tube due to the pressure field which would remain if the local swirling velocity were removed. This is given by

$$-\nabla P_{\mathrm{B}} = \rho(\partial \boldsymbol{V}_{\mathrm{B}}/\partial t + (\boldsymbol{V}_{\mathrm{B}} - \boldsymbol{V})\cdot\nabla \boldsymbol{V}_{\mathrm{B}}). \tag{2.7}$$

The right-hand side of (2.7) is the acceleration of a particle which moves with the velocity $\boldsymbol{V}_{\mathrm{B}}$. The second term on the right-hand side is added because $\partial \boldsymbol{V}_{\mathrm{B}}/\partial t$ is the acceleration seen by an observer moving with velocity $\boldsymbol{V}$, not $\boldsymbol{V}_{\mathrm{B}}$. This will be further approximated by neglecting the transverse part of the gradient of $\boldsymbol{V}_{\mathrm{B}}$ which is unknown. Thus we use

$$-\nabla P_{\mathrm{B}} = \rho(\partial \boldsymbol{V}_{\mathrm{B}}/\partial t - \boldsymbol{u}\cdot\hat{\boldsymbol{t}}\,\partial \boldsymbol{V}_{\mathrm{B}}/\partial \xi). \tag{2.8}$$

All of the terms on the right-hand side of (2.3) represent terms which appear in the MS external force expressions, MS(4.11) or MS(5.18). Moore & Saffman made an additional restriction to flows which are slowly varying in time in addition to the small curvature assumption. Because of this, all but the Kutta–Joukowsky lift term were found to be small and were neglected by them. We, however, will retain these terms. For this reason (2.3) should be thought of as a model equation rather than the result of asymptotic analysis. Among the reasons for exploring this model system is the fact that the axial force term can be balanced by axial acceleration even on a straight vortex. These so-called 'fast' terms which were neglected in the MS formulation are the necessary terms for existence of axial waves as will be shown in §4. Other terms which we have kept are important for the growth rate of helical instabilities and other rapid transverse motions. The validity and/or interest in this model should be decided by comparison with experiments such as vortex breakdown phenomena.

There are other differences between (2.3) and the MS formulation which will be apparent to the reader who compares this equation with MS(5.18), for the external forces, and MS(6.7), which contains the inertial terms and internal pressure forces.

The differences occur essentially because their material derivative is with respect to a particle which moves with the vortex but does not slide along it with the axial flow. This means that even for uniform axial flow there are contributions from momentum integral terms which do not appear explicitly in (2.3) but are contained in the acceleration on the left-hand side of the equation.

Now denote the local relative velocity by $\boldsymbol{u} = \boldsymbol{V} - \boldsymbol{V}_{\mathrm{B}}$. Equation (2.3) may then be written

$$\rho A \frac{\partial \boldsymbol{u}}{\partial t} = -\rho A \left(\frac{\partial \boldsymbol{u}_{\mathrm{T}}}{\partial t} - \boldsymbol{u} \cdot \hat{\boldsymbol{t}} \frac{\partial \boldsymbol{u}_{\mathrm{T}}}{\partial s} \right) + \rho \Gamma \hat{\boldsymbol{t}} \times \boldsymbol{u} - \left(\frac{\rho \Gamma^2}{8\pi A} \right) \frac{\partial A}{\partial s} \hat{\boldsymbol{t}} - \rho A \boldsymbol{u} \cdot \hat{\boldsymbol{t}} \frac{\partial \boldsymbol{V}_{\mathrm{B}}}{\partial s}. \tag{2.9}$$

The final forms of the equations to determine the vortex shape and area distribution are

$$\partial \boldsymbol{r} / \partial t = \boldsymbol{V}_{\mathrm{B}} + \boldsymbol{u}, \tag{2.10}$$

$$\frac{\partial (2\boldsymbol{u} - \boldsymbol{u} \cdot \hat{\boldsymbol{t}}\hat{\boldsymbol{t}})}{\partial t} = (\boldsymbol{u} \cdot \hat{\boldsymbol{t}}/\lambda) \frac{\partial (\boldsymbol{u} - \boldsymbol{u} \cdot \hat{\boldsymbol{t}}\hat{\boldsymbol{t}} - \boldsymbol{V}_{\mathrm{B}})}{\partial \xi} + \left(\frac{\Gamma \lambda}{A_0} \right) \hat{\boldsymbol{t}} \times \boldsymbol{u} + \left(\frac{\Gamma^2}{8\pi A_0} \right) \frac{\partial \ln (\lambda)}{\partial \xi} \hat{\boldsymbol{t}}, \tag{2.11}$$

$$\hat{\boldsymbol{t}} = \frac{1}{\lambda} \frac{\partial \boldsymbol{r}}{\partial \xi}, \tag{2.12}$$

$$\lambda = |\partial \boldsymbol{r} / \partial \xi|, \tag{2.13}$$

$$\lambda A = A_0. \tag{2.14}$$

All the spatial derivatives have been expressed as ξ derivatives. Equation (2.11) is an evolution equation for $2\boldsymbol{u} - \boldsymbol{u} \cdot \hat{\boldsymbol{t}}\hat{\boldsymbol{t}} (= \boldsymbol{R})$ from which $\boldsymbol{u}$ itself may be computed by $\boldsymbol{u} = \frac{1}{2}(\boldsymbol{R} + \boldsymbol{R} \cdot \hat{\boldsymbol{t}}\hat{\boldsymbol{t}})$. An evolution equation for λ (or A) is obtained by differentiating (2.13) with respect to time and using (2.10). This is

$$\partial \lambda / \partial t = \hat{\boldsymbol{t}} \cdot \partial (\boldsymbol{V}_{\mathrm{B}} + \boldsymbol{u}) / \partial \xi. \tag{2.15}$$

3. Intrinsic equations

The equations derived in §2 may be cast in an intrinsic form which is useful for comparison with other work, in particular they generalize intrinsic equations derived by Betchov (1965) for the motion of vortex tubes without axial flow and with a Biot–Savart interaction truncated to the local induction approximation. A local orthogonal coordinate system is introduced along the vortex centreline consisting of the tangent $\hat{\boldsymbol{t}}$, the normal $\hat{\boldsymbol{n}}$ and the binormal $\hat{\boldsymbol{b}}$ which vary along the vortex according to the Frenet–Serret formulae

$$\partial \hat{\boldsymbol{t}} / \partial s = \kappa \hat{\boldsymbol{n}}, \tag{3.1}$$

$$\partial \hat{\boldsymbol{n}} / \partial s = -\kappa \hat{\boldsymbol{t}} + \tau \hat{\boldsymbol{b}}, \tag{3.2}$$

$$\partial \hat{\boldsymbol{b}} / \partial s = -\tau \hat{\boldsymbol{n}}, \tag{3.3}$$

where κ and τ are the local curvature and torsion. The velocities are represented locally by

$$\boldsymbol{V}_{\mathrm{B}} = W_{\mathrm{B}} \hat{\boldsymbol{t}} + U_{\mathrm{B}} \hat{\boldsymbol{n}} + V_{\mathrm{B}} \hat{\boldsymbol{b}}, \tag{3.4}$$

and

$$\boldsymbol{v} = w\hat{\boldsymbol{t}} + u\hat{\boldsymbol{n}} + v\hat{\boldsymbol{b}}. \tag{3.5}$$

The objective is to find equations for the evolution of u, v, w, λ, κ, τ without regard for the position of the vortex tube in space. The derivation, which is sketched in Appendix A, yields the following equations,

$$\frac{\partial \lambda}{\partial t} = \frac{\partial (W_B + w)}{\partial \xi} - (U_B + u)\lambda\kappa, \tag{3.6}$$

$$\frac{\partial (\lambda\kappa)}{\partial t} = \frac{\partial A_1}{\partial \xi} - A_2 \tau\lambda, \tag{3.7}$$

$$\frac{\partial (\lambda\tau)}{\partial t} = \frac{\partial B_1}{\partial \xi} + A_2 \kappa\lambda, \tag{3.8}$$

$$\frac{\partial w}{\partial t} = 2A_1 u + 2A_2 v - wu\kappa - w\lambda^{-1}\frac{\partial W_B}{\partial \xi} + wU_B\kappa + \frac{\Gamma^2}{8\pi A_0}\frac{\partial \ln(\lambda)}{\partial \xi}, \tag{3.9}$$

$$2\frac{\partial u}{\partial t} = -A_1 w + 2B_1 v - wv\tau + w\lambda^{-1}\frac{\partial u}{\partial \xi} - w\lambda^{-1}\frac{\partial U_B}{\partial \xi} - wW_B\kappa + wV_B\tau - \left(\frac{\Gamma\lambda}{A_0}\right)v, \tag{3.10}$$

$$2\frac{\partial v}{\partial t} = -A_2 w - 2B_1 u + wu\tau + w\lambda^{-1}\frac{\partial v}{\partial \xi} - w\lambda^{-1}\frac{\partial V_B}{\partial \xi} - wU_B\tau + \left(\frac{\Gamma\lambda}{A_0}\right)u, \tag{3.11}$$

where

$$A_1 = (W_B + w)\kappa + \lambda^{-1}\frac{\partial (U_B + u)}{\partial \xi} - (V_B + v)\tau, \tag{3.12}$$

$$A_2 = (U_B + u)\tau + \lambda^{-1}\frac{\partial (V_B + v)}{\partial \xi}, \tag{3.13}$$

$$B_1 = \frac{A_1\tau}{\kappa} + (\lambda\kappa)^{-1}\frac{\partial A_2}{\partial \xi}. \tag{3.14}$$

These equations are completely equivalent to those presented in §2. However, they are not independent equations for the set u, v, w, λ, κ, τ, in general, because the Biot–Savart velocity components are not functions of λ, κ, τ alone, but depend on other aspects of the geometry as well. The special cases of vortex rings and helices of constant area which are described by this limited set are presented below.

The intrinsic equations can also be used with the local induction approximation where the Biot–Savart velocities defined by (3.4) are approximated by ($U_B = 0$, $V_B = (\Gamma\kappa/4\pi)K$, $W_B = 0$) where the local-induction parameter $K = [\ln(1/\kappa\sigma) + C]$ is usually further approximated as a constant. In the latter approximation the Biot–Savart components depend only on the local curvature, and the intrinsic equations form a closed set.

3.1. *Ring example*

As an example of the utility of the intrinsic equations consider a uniform vortex ring with axial flow. While this may appear to be an academic example, it may be possible to generate one in a modified vortex generator in which the cylinder housing the generator piston is caused to rotate rapidly just as the piston is driven to create the vortex ring. For a vortex ring with axial flow

$$W_B = 0,$$

$$U_B = 0,$$

$$V_B = (\Gamma\kappa/4\pi)[\ln(8/\kappa\sigma) - \tfrac{1}{2} + \tfrac{1}{4}\mu_s], \tag{3.15}$$

where $\mu_s = 1$ for uniform vorticity and $\mu_s = 0$ for a hollow vortex. Since $\tau = 0$ and λ, κ, u, v, w are all independent of ξ, it follows that $A_2 = 0$, $B_1 = 0$ and $A_1 = w\kappa$ and the equations reduce to

$$\mathrm{d}\lambda/\mathrm{d}t = -u\lambda\kappa, \tag{3.16}$$

$$\mathrm{d}(\lambda\kappa)/\mathrm{d}t = 0, \tag{3.17}$$

$$\mathrm{d}w/\mathrm{d}t = uw\kappa, \tag{3.18}$$

$$\mathrm{d}u/\mathrm{d}t = -0.5w^2\kappa - (\Gamma\lambda/2A_0)\,v, \tag{3.19}$$

$$\mathrm{d}v/\mathrm{d}t = (\Gamma\lambda/2A_0)\,u. \tag{3.20}$$

There is a steady solution in which $u = 0$, $w =$ constant and

$$v = -\kappa A_0 w^2/\Gamma \tag{3.21}$$

which is in agreement with Widnall & Bliss (1971). The forward speed of the ring is $V_B + v$. The effect of the axial flow is to cause the vortex to slow down from the induced Biot–Savart velocity in order for the Kutta–Joukowsky lift in the resulting cross-flow to balance the centrifugal force.

There is an interesting transient problem. Suppose that a vortex ring of initial radius R_0, axial velocity w_0 and area $A_0 (= \pi\sigma_0^2)$ is started with $u = v = 0$ so that the initially unbalanced centrifugal force requires radial acceleration. The above equations then describe how the motion evolves in time. It will be shown that the velocity doesn't tend to the steady state value (3.21), but instead oscillates about it.

Since $\lambda = R/R_0$ and $\kappa = 1/R$, (3.17) is identically satisfied, and (3.16) becomes

$$\mathrm{d}R/\mathrm{d}t = -u. \tag{3.22}$$

From (3.18) and (3.22) an integral

$$wR = w_0 R_0, \tag{3.23}$$

is found which expresses conservation of angular momentum around the ring. Another integral can be found from (3.20) and (3.22), namely

$$v = -(\Gamma R_0/4A_0)(R^2/R_0^2 - 1). \tag{3.24}$$

Substituting (3.22), (3.23) and (3.24) into (3.19) gives a differential equation for R:

$$\mathrm{d}^2R/\mathrm{d}t^2 = 0.5w_0^2R_0^2/R^3 - 0.5(\Gamma/2A_0)^2R(R^2/R_0^2 - 1). \tag{3.25}$$

This can be put in a convenient dimensionless form by introducing $v_0 = \Gamma/2\pi\sigma_0$ and $t_0 = \sigma_0/v_0$, the latter being proportional to the turn around time of the vortex. Now defining

$$\tilde{t} = t/t_0, \tag{3.26}$$

$$\epsilon = (w_0^2/v_0^2)(\sigma_0^2/R_0^2), \tag{3.27}$$

and

$$(R/R_0) - 1 = \epsilon f, \tag{3.28}$$

where ϵ is a small parameter, (3.25) may be written

$$\partial^2 f/\partial\tilde{t}^2 = 0.5(1+\epsilon f)^{-3} - 0.5f(1+\epsilon f)(2+\epsilon f). \tag{3.29}$$

When terms of order ϵ on the right-hand side are neglected the solution is $f = 0.5[1-\cos(\tilde{t})]$, or

$$(R/R_0) = 1+0.5\epsilon[1-\cos(\tilde{t})]. \tag{3.30}$$

From (3.24) it follows that

$$v = -(A_0 w_0^2/R_0\Gamma)[1-\cos(\tilde{t})]. \tag{3.31}$$

Therefore the solution oscillates about the steady state solution and, while the radius of the ring varies by only a very small amount, the oscillation is at such a high frequency that the velocity varies by an amount comparable to the Biot–Savart velocity when w_0 is comparable to v_0. This can be seen more clearly when the result for the forward speed is written

$$V_B+v = (\Gamma/4\pi R_0)\{\ln(8R_0/\sigma_0)-\tfrac{1}{2}+\mu_s/4-(w_0^2/v_0^2)[1-\cos(\tilde{t})]\}, \tag{3.32}$$

neglecting terms of order ϵ.

3.2. *Helix example*

A second example is provided by a uniform helix with axial flow. At a particular instant the helix has shape

$$\boldsymbol{r} = D\hat{\boldsymbol{r}}(\theta)+z\hat{\boldsymbol{k}} \quad (\theta = -\gamma z), \tag{3.33}$$

in cylindrical coordinates. This is a right-handed helix with respect to the z-direction when the wavenumber γ is negative, left-handed when γ is positive. In cylindrical coordinates the geometric parameters are

$$\hat{\boldsymbol{t}} = (-D\gamma\hat{\boldsymbol{\theta}}+\hat{\boldsymbol{k}})/(1+\gamma^2D^2)^{\frac{1}{2}}, \tag{3.34}$$

$$\hat{\boldsymbol{n}} = -\hat{\boldsymbol{r}}, \tag{3.35}$$

$$\hat{\boldsymbol{b}} = (-\gamma D\hat{\boldsymbol{k}}-\hat{\boldsymbol{\theta}})/(1+\gamma^2D^2)^{\frac{1}{2}}, \tag{3.36}$$

and

$$\kappa = D\gamma^2/(1+\gamma^2D^2), \quad \tau = -\gamma(1+\gamma^2D^2). \tag{3.37}$$

In the intrinsic coordinate system the Biot–Savart velocity has non-zero components V_B and W_B, however simple expressions are only known (Kelvin 1880) for a helix of small pitch, γD, and uniform vorticity in which case $W_B = O(\Gamma\gamma^3D^2)$ and

$$V_B = \frac{\Gamma\gamma^2DK}{4\pi}, \quad K = \ln\left(\frac{2}{|\gamma|\sigma}\right)-C+\tfrac{1}{4}, \quad C = 0.577\ldots. \tag{3.38}$$

For a uniform helix (not necessarily of small pitch) the intrinsic equations are

$$\mathrm{d}\lambda/\mathrm{d}t = -u\gamma\kappa, \tag{3.39}$$

$$\mathrm{d}(\lambda\kappa)/\mathrm{d}t = -u\tau^2\lambda, \tag{3.40}$$

$$\mathrm{d}(\lambda\tau)/\mathrm{d}t = u\tau\kappa\lambda, \tag{3.41}$$

$$\mathrm{d}w/\mathrm{d}t = 2A_1u+2uw\tau-wu\kappa, \tag{3.42}$$

$$2\,\mathrm{d}u/\mathrm{d}t = -A_1w+2B_1v-wv\tau+w(V_B\tau-W_B\kappa)-(\Gamma\lambda/A_0)v, \tag{3.43}$$

$$2\,\mathrm{d}v/\mathrm{d}t = -2B_1u+(\Gamma\lambda/A_0)u, \tag{3.44}$$

with

$$A_1 = (W_B+w)\kappa-(V_B+v)\tau, \quad B_1 = A_1\tau/\kappa. \tag{3.45}$$

In general these equations have a steady solution in which $u = 0$, $\lambda = 1$ and κ, τ, w, v are constants, provided that the right-hand side of (3.43), which is quadratic in v, has real roots. These roots give the solution

$$v/v_0 = (\kappa/2\tau^2\sigma_0)\{\beta+\alpha-1\pm[2+2\alpha^2-(\beta+\alpha+1)^2]^{\frac{1}{2}}\}, \tag{3.46}$$

where $$\beta = \left(\frac{w}{v_0}\right)\tau\sigma_0, \quad \alpha = \left(\frac{W_B}{v_0}\right)\tau\sigma_0 - \left(\frac{V_B}{v_0}\right)\frac{\tau^2\sigma_0}{\kappa}, \quad v_0 = \frac{\Gamma}{2\pi\sigma_0}.$$

The condition that (3.46) be real is

$$-1-\alpha-(2+2\alpha^2)^{\frac{1}{2}} < \beta < -1-\alpha+(2+2\alpha^2)^{\frac{1}{2}}. \tag{3.47}$$

When β is positive (negative) the solution takes the form of a right-handed (left-handed) helix when w is positive and of the opposite handedness when it is negative. Stability of this solution may be tested as follows. Equations (3.39), (3.40) and (3.41) may be manipulated to show that $\mathrm{d}D/\mathrm{d}t = -u$. Using this, (3.43) may be written

$$\mathrm{d}^2D/\mathrm{d}t^2 = QD, \tag{3.48}$$

where Q is the quantity v/D. If (3.47) is satisfied, v/D lies between the two real roots of Q and Q is negative. If 3.47 is violated there are no real roots and Q is positive. Linearization about the steady solution then shows stability if (3.47) is satisfied and exponential growth from any initial condition if it is not. These results will be compared below with other known results.

Assuming small pitch and using (3.38) an expansion can be carried out in powers of $\gamma\delta_0$ with D/σ_0, v/v_0 and w/v_0 of order one. Equation (3.46) then gives (with the positive sign)

$$\frac{v}{v_0} = -0.5\left(\frac{w}{v_0}\right)^2\left(\frac{D}{\sigma_0}\right)(\gamma\sigma_0)^2 + 0.5\left(\frac{w}{v_0}\right)^2\left(\frac{D}{\sigma_0}\right)(\gamma\sigma_0)^3 - 0.5\left(\frac{w}{v_0}\right)\left(\frac{D}{\sigma_0}\right)(\gamma\sigma_0)^3K + O(\gamma\sigma_0)^4. \tag{3.49}$$

This is not in complete agreement with MS who give an exact result from linear theory when $D \ll \sigma_0$. For uniform axial flow and uniform vorticity there should be an additional third-order term, $-0.25(w/v_0)(D/\sigma_0)(\gamma\sigma_0)^3$ in (3.49). This has been traced to the neglected profile dependent momentum integral in (2.2). The missing term results from the flux of the swirling part of the flow through the control surface by the non-uniform axial velocity of the control surface as it follows the curved centreline. For a hollow vortex this term would be zero, and of course it is zero for the slightly non-uniform slug flow mentioned in §2, for any swirl profile.

The second solution from (3.46) (the negative sign) expands with a first term of order one, $v/v_0 = -D/\sigma_0 + \ldots$. Both solutions are stable (to helical disturbances of the same wavelength) by the reasoning above.

There is another formal expansion of (3.46) in powers of $\gamma\sigma_0$ in which D/σ_0, v/v_0 and $\beta(=-\gamma\sigma_0 w/v_0)$ are of order one. Notice that β has been redefined here for small $\gamma\sigma_0$. When β is of order one and $\gamma\sigma_0$ is small this means that w/v_0 must be large. To lowest order this expansion gives

$$v/v_0 = (D/2\sigma_0)[\beta-1\pm(1-2\beta-\beta^2)^{\frac{1}{2}}]. \tag{3.50}$$

This is a real solution if $-1-\sqrt{2} < \beta < -1+\sqrt{2}$ and is stable in this range. Equation (3.50), which is a finite amplitude result, is also a solution in the limit as

$D \to 0$ (a straight vortex) for any value of β. This solution is unstable when the inequality is violated. The result says that the straight vortex is unstable when

$$\gamma\sigma_0 w/v_0 > 1+\sqrt{2}, \tag{3.51}$$

with the instability taking the form of a left-handed helix when w is positive, right-handed when w is negative. The other inequality describes a more unstable situation, with the instability occurring when

$$-\gamma\sigma_0 w/v_0 > -1+\sqrt{2}, \tag{3.52}$$

in the form of a right-handed helix when w is positive, left-handed when it is negative. Equations (3.51) and (3.52) agree with results of WB and MS.

Another source for comparison are the linear stability computations of Lessen, Deshpande & Hadji-Ohanes (1973) for hollow and uniform vortices with 'top-hat' axial flow. When the above inequalities are corrected through terms of order $(\gamma\sigma_0)^{-2}$, which can be deduced from (3.47), they agree with the hollow vortex results to within about 10%, even for $\gamma\sigma_0$ as large as one. For the uniform vortex we can say the same, except the available computations to compare with (3.52) are limited to small $\gamma\sigma_0$.

Lessen, Singh & Paillet (1974) have also done a stability study of vortices with Gaussian axial flow which shows that the stability of the helical modes is profile dependent. The results show that (3.52) is approximately satisfied with 0.2 on the right-hand side instead of $-1+\sqrt{2}$ so we could say that our result is qualitatively correct. However there is a more important difference. Lessen's helical mode becomes stable again for larger wavenumbers, for wavelengths comparable to the jet radius. There is a band of instability which becomes narrower as w/v_0 becomes smaller, until there is complete stability for w/v_0 smaller than about 0.66. This shows that our results are qualitatively correct for a large enough value of the axial flow.

It is interesting to speculate about the behaviour of the unstable helix when the amplitude (D) becomes large. We have therefore solved the intrinsic helix equations numerically, in the local induction approximation, starting from $u = v = 0$, $w = w_0$ and an initially small value of D. The results show that in the unstable range the resulting motion is periodic, with D oscillating between the initial value and a maximum of order σ_0. The maximum is larger and the period shorter when the initial conditions are further into the unstable range, for fixed γ. The axial velocity and torsion become smaller as D nears its maximum in such a way that the quantity β, defined in (3.46), penetrates back into the stable range given by (3.47) and prevents further growth. A surprising observation is that the results are only slightly dependent on the Biot–Savart velocity if the self induction constant is not too large. That is, the computational results are nearly the same when V_B is set to zero. This means that the inertial forces and cross-flow lift are dominant when there is axial flow. Also note that when the Biot–Savart components are neglected $\alpha = 0$ in (3.47). If one checks back to the ring example it will be seen that the Biot–Savart velocity did not actually appear in those equations. This suggests that insight could result from studying the general intrinsic equations (3.6)–(3.14), with all of the Biot–Savart components neglected. One might call this the 'no-induction' approximation.

4. One-dimensional flow. Vortex breakdown

One-dimensional flow will illustrate the dynamical effect of area variation along a vortex tube. Consider the case where the vortex is aligned along the z-axis. Then $s = z$, $\hat{\boldsymbol{t}} = \hat{\boldsymbol{k}}$ and $V_B = 0$. The Lagrangian equations reduce to

$$\partial z/\partial t = w, \tag{4.1}$$

$$\partial w/\partial t = (\Gamma^2/8\pi A_0)\,\partial \ln(\lambda)/\partial \xi, \tag{4.2}$$

$$\partial \lambda/\partial t = \partial w/\partial \xi, \tag{4.3}$$

$$\lambda = \partial z/\partial \xi. \tag{4.4}$$

It is a simple matter to convert these to the more familiar Eulerian form by replacing the material derivative by $\partial/\partial t + w\,\partial/\partial z$, where $\partial/\partial t$ here is understood to be taken with z held fixed, and using (4.4) to convert from ξ to z derivatives. With A as the dependent variable instead of λ the resulting equations are

$$\partial A/\partial t + \partial A w/\partial z = 0, \tag{4.5}$$

$$A(\partial w/\partial t + w\,\partial w/\partial z) = -\partial(\Gamma^2 \ln(A)/8\pi)/\partial z. \tag{4.6}$$

These are the same as the equations of one-dimensional isentropic gas dynamics with A the 'density' and $\Gamma^2 \ln(A)/8\pi$ the 'pressure'. Therefore the motion consists of waves propagating to the right and left relative to the fluid with 'sound speed' c defined by

$$c^2 = \frac{d\text{ 'pressure'}}{d\text{ 'density'}} = \frac{\Gamma^2}{8\pi A}. \tag{4.7}$$

Since the maximum local swirl velocity for a sharp-edged vortex is given by

$$V_{\max} = \Gamma/2\pi\sigma, \tag{4.8}$$

this result says that $c = V_{\max}/\sqrt{2}$. When the vortex is not sharp edged, $V_{\max}$ is defined by (4.8).

The vortex equations have a closer analogy with the flow of shallow water because neither water nor vortex system have an internal energy equation. In this analogy the vortex tube area A corresponds to the water depth. In the shallow-water approximation (Whitham 1974) the vertical acceleration is neglected, the pressure being determined from the hydrostatic pressure alone. Equations (4.5) and (4.6) may be derived from a 'shallow-water' approximation in which the radial pressure gradient in the vortex tube is balanced locally by the centrifugal forces of the swirling flow. The analogy is even closer if one looks at the characteristic form of (4.5) and (4.6). The characteristic equations are

$$\left.\begin{aligned} C_+ &: \quad w - 2c = \text{constant along } \mathrm{d}z/\mathrm{d}t = w + c, \\ C_- &: \quad w + 2c = \text{constant along } \mathrm{d}z/\mathrm{d}t = w - c. \end{aligned}\right\} \tag{4.9}$$

These are the same as for shallow water, or gas dynamics with specific heats ratio equal to 2, except with c defined by (4.7). (For shallow water $c = (gh)^{\frac{1}{2}}$.)

As for water waves, vortex waves will steepen and ultimately break on the front side of a wave of enlargement (a locally swollen core). The basic equations have weak solutions with shock discontinuities which conserve mass and momentum in analogy

with bores in water. According to Whitham (1974) the shock jump conditions may be written

$$W[A] = [Aw], \tag{4.10}$$

$$W[Aw] = [Aw^2 + (\Gamma^2/8\pi)\ln(A)], \tag{4.11}$$

where [ ] indicates the jump in a quantity across the shock and W is the shock propagation speed. From these one finds that a right (left) travelling shock with a region of area A_2 propagating into a region of smaller area A_1 has velocity of propagation

$$W = w_1 \pm c_1\{\ln(A_2/A_1)/(1-A_1/A_2)\}^{\frac{1}{2}} \tag{4.12}$$

and the fluid velocity behind the front is

$$w_2 = w_1 \pm (1-A_1/A_2)\, c_1\{\ln(A_2/A_1)/(1-A_1/A_2)\}^{\frac{1}{2}}. \tag{4.13}$$

Since the bracketed quantity is always greater than 1, the shock propagates with supersonic speed relative to the state in front, as it should. Equation (4.12) gives the relative Mach number versus the area ratio. The inverse of this corresponds to density ratio versus Mach number, one of the well-known shock relations of gas dynamics. Equation (4.13) could be rearranged to give the Mach number behind the shock.

The shallow-water approximations, being long-wave approximations, cease to be valid when axial derivatives are no longer small. However, breaking does occur in water and the shallow-water theory gives a satisfactory description of bores and hydraulic jumps (steady bores). Because of the strong analogy one might expect similar success for vortex waves. The shock-like discontinuity described above appears to describe the phenomenon known as vortex breakdown. The shock structure of vortex breakdown has been investigated experimentally by Sarpkaya (1971) and Faler & Leibovich (1978) and others (Leibovich 1978). The structure is several core diameters long and, in a stationary frame, contains a stagnation point and a rather distinct annular recirculation bubble which superficially resembles the roller which occurs in strong hydraulic jumps. Often vortex breakdown is followed by a spiralling disturbance which becomes turbulent. Leibovich (1978) and Escudier, Bornstein & Maxworthy (1982) ascribe this phenomenon to the unstable growth of helical disturbances on the jet-like (or wake-like) axial flow behind the breakdown, a point of view which will be seen to be consistent with the present work.

The most complete theoretical formulation of vortex breakdown is that of Benjamin (1962, 1967), who pursued an analogy with weak undular bores in which the process is assumed to be both steady and non-dissipative. In contrast the unsteady breaking waves described above terminate in a vortex breakdown description which has its analogue with the Rayleigh theory of strong bores (Lamb 1932), a process in which there is an energy loss. The present equations are non-dispersive, however, and cannot describe the undulations observed behind a weak vortex breakdown, nor can they describe a non-breaking solitary wave, without including additional terms to represent the neglected radial acceleration.

Comparison may be made between the present theory and a simple example of Benjamin's theory which appears not to have been noticed before: a hollow potential vortex with uniform axial flow in the core provides co-conjugate states for

Benjamin's theory. The details of this are outlined in Appendix B and put in a form comparable with (4.12) and (4.13). These results are

$$W = w_1 \pm V_{1\max}(1+A_1/A_2)^{-\frac{1}{2}}, \tag{4.14}$$

$$w_2 = w_1 \pm (1-A_1/A_2)\, V_{1\max}(1+A_1/A_2)^{-\frac{1}{2}}, \tag{4.15}$$

where $V_{1\max}$ is defined by (4.8). These are in agreement with (4.12) and (4.13) for weak breakdowns, being the same to first and second order, respectively, in the small quantity $(1-A_1/A_2)$ and differing by only about 5% for an area ratio of 4 and about 15% for an area ratio of 10. In particular both methods give $V_{\max}/\sqrt{2}$ as the limiting value of the shock speed as the shock strength tends to zero. The close agreement may not persist for other pairs of conjugate states.

A comparison may also be made with a wave speed computation of Maxworthy, Mory & Hopfinger (1983). Using Benjamin's (1967) perturbation method with a Burgers vortex swirl profile and approximately Gaussian axial flow, with parameters selected to agree with experiment, they computed the wave speed for weak waves propagating with or against the stream. The results were $0.93W_{\mathrm{m}} \pm 0.72V_{\max}$, where W_{m} is the maximum axial velocity and $V_{\max}$ is *not* the maximum swirl velocity in their profile, but is defined in terms of Γ as above. Comparing this with the results of the present analysis, $w \pm 0.707V_{\max}$, suggests only a weak dependence on the details of the swirl and axial profiles.

Direct comparison may be made with experimental vortex breakdown results of Leibovich (1978) and Garg & Leibovich (1979). They have presented results for six stationary vortex breakdown flows in a vortex generator device. The axial and swirl velocities were found to be represented by

$$w = W_{\mathrm{A}} + W_{\mathrm{B}} \exp(-\alpha r^2), \tag{4.16}$$

$$v_\theta = K \exp(-\alpha r^2)/r, \tag{4.17}$$

in both the region upstream of the breakdown where the axial profile is jet-like ($W_{\mathrm{B}} > 0$) and downstream where the profile is wake-like ($W_{\mathrm{B}} < 0$). In each of the flows they give values for W_{A}, W_{B}, α and K. In our configuration this corresponds to a left travelling shock with a superimposed uniform velocity to the right which makes the shock stationary. In order to compare we will assume that their maximum velocity W_{B} is the same as our average velocity. This gives us a way to define the radius σ, i.e.

$$\pi\sigma^2 = \int_0^\infty \exp(-\alpha r^2)\, 2\pi r^2 \, \mathrm{d}r \tag{4.18}$$

gives

$$\sigma = \alpha^{-\frac{1}{2}}. \tag{4.19}$$

The quantity K is $\Gamma/2\pi$, therefore our defined quantity $V_{\max} = \Gamma/2\pi\sigma = K\alpha^{\frac{1}{2}}$. The shock speed was taken as the negative of the value of W_{A} at the axial position of the stagnation point. This had to be determined by interpolation since the flow was in a slightly divergent tube. Thus the quantities $w_1/V_{1\max}$, $w_2/V_{1\max}$, $W/V_{1\max}$ and A_2/A_1 were determined from the experiments and used to calculate values of $(W-w_1)/V_{1\max}$ and $(w_2-w_1)/V_{1\max}$ versus A_2/A_1 for comparison with (4.12) and (4.13). These results are shown in figures 1(*a*) and 1(*b*) where the agreement is seen to be remarkably good. The other things to notice are that the area ratio across a breakdown can be quite large and that the spiral type breakdown occurs for smaller area ratios, i.e. these are weaker shocks.

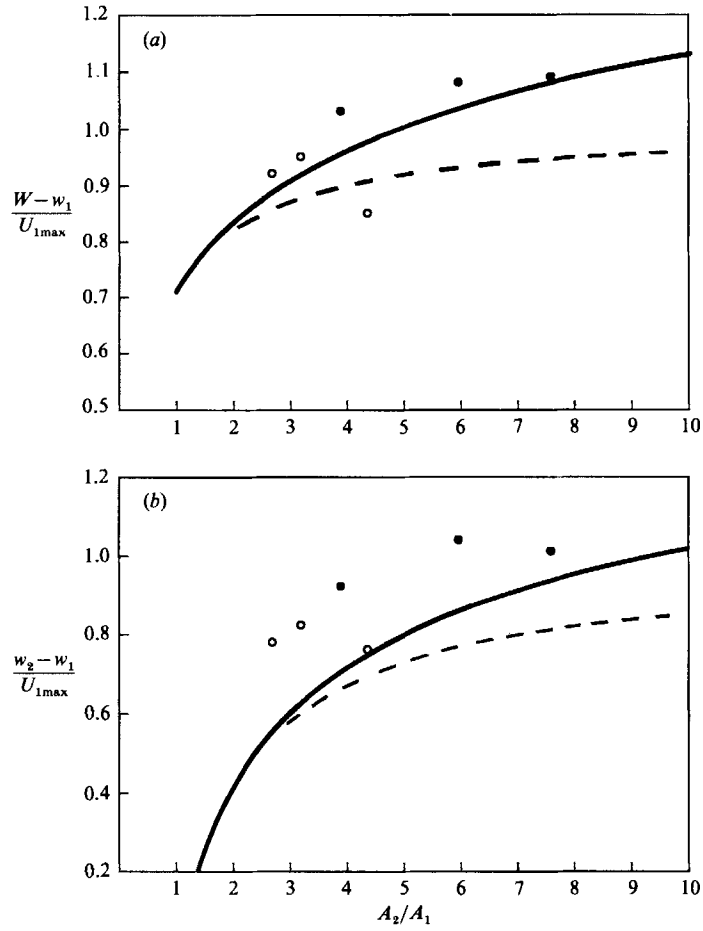

FIGURE 1. Shock jump conditions in vortex breakdown. The experimental points are from Garg & Leibovich. ●, bubble breakdowns; ○, spiral breakdowns; ——, present theory; – – –, Benjamin's theory for a hollow vortex, (4.14) and (4.15). (*a*) Shock speed relative to the upstream state divided by the upstream swirl velocity versus area ratio across the shock. (*b*) Velocity difference across the shock divided by upstream swirl.

A sample computation has been carried out with the Lagrangian form of the equations, (4.2) and (4.3), expressed in conservation form in order to accurately capture shocks. When programmed in conservation form the shock jump conditions (4.10) and (4.11) will automatically be satisfied. A modified Godunov method was used (Van Leer 1979) with spatial increments equal to σ_0. The initial conditions were chosen to be similar to those in a vortex dynamics experiment reported by Leonard (1985) in which a hollow vortex with a section of axial flow was simulated by using six vortex filaments initially arranged on the surface of a cylinder, wound into a helical pattern on one part in order to give axial flow. In addition a seventh vortex of the same strength extended along the axis. In the present computation the initial core radius was σ_0 and w was taken negative on a section of length $20\sigma_0$ in a parabolic manner with maximum velocity equal to the maximum swirl velocity, and zero elsewhere. Equation (4.1) was solved simultaneously in order to plot the results versus z. Figure 2(*a*) shows the core variation after 2 time units (2π units are one

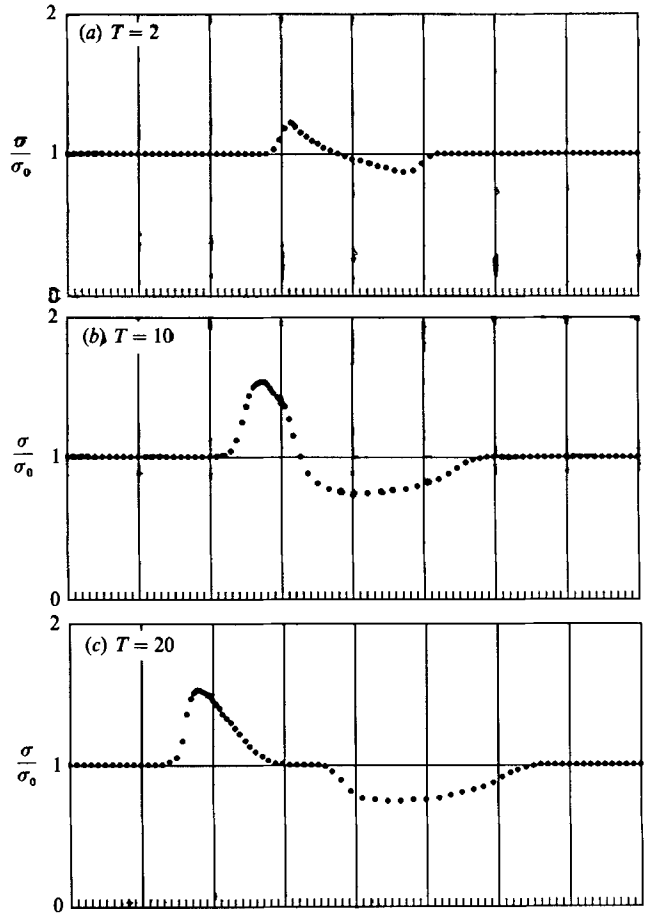

FIGURE 2. Waves on a straight vortex tube in a numerical experiment. Core radius versus axial distance both normalized by the upstream core radius.

turn-around-time of the vortex). Figure 2 (*b*) shows the core radius after 10 time units which corresponds to the final time in Leonard's figure 11 (*b*). There is a similarity in the results with enlargement on the left and contraction on the right. Figure 2 (*c*) is at 20 time units. It shows complete separation of two simple waves (the Riemann invariant $w-2c$ is constant in the left travelling wave and the Riemann invariant $w+2c$ is constant in the right travelling wave). A wave of enlargement propagates to the left steepening into a vortex breakdown on its front side (it is no longer a simple wave after breaking), while a wave of contraction propagates to the right steepening into a vortex breakdown on its back side. The vortex breakdowns do not develop into sharp discontinuities because of numerical viscosity introduced by the difference approximation. At later times the waves continue to separate with relatively small change of shape.

5. Three-dimensional flow. The growth of helical waves

The basic Lagrangian equations, (2.10)–(2.15), have been programmed using MacCormack's (1971) method. This is essentially a two-step Runge–Kutta method in

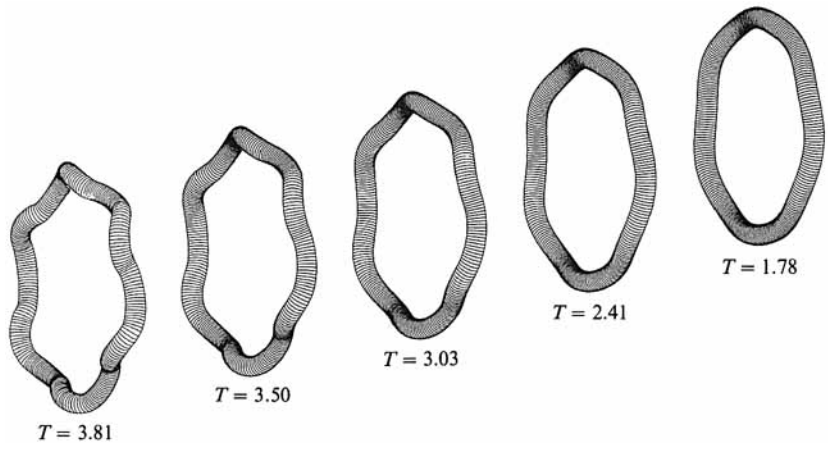

FIGURE 3. Perspective views of growing helical disturbance on a vortex ring. The vortex ring of radius $10\sigma_0$ with axial velocity $w = 2V_{max}$ was initially in the (y,z)-plane. It was perturbed out of plane by $x = 0.1\sigma_0 \sin n\theta$ with $n = 6$. The viewpoint of the ring is from $x = 50\sigma_0$, $y = -86\sigma_0$, $z = 0$ (x out of page, y to the right, z up).

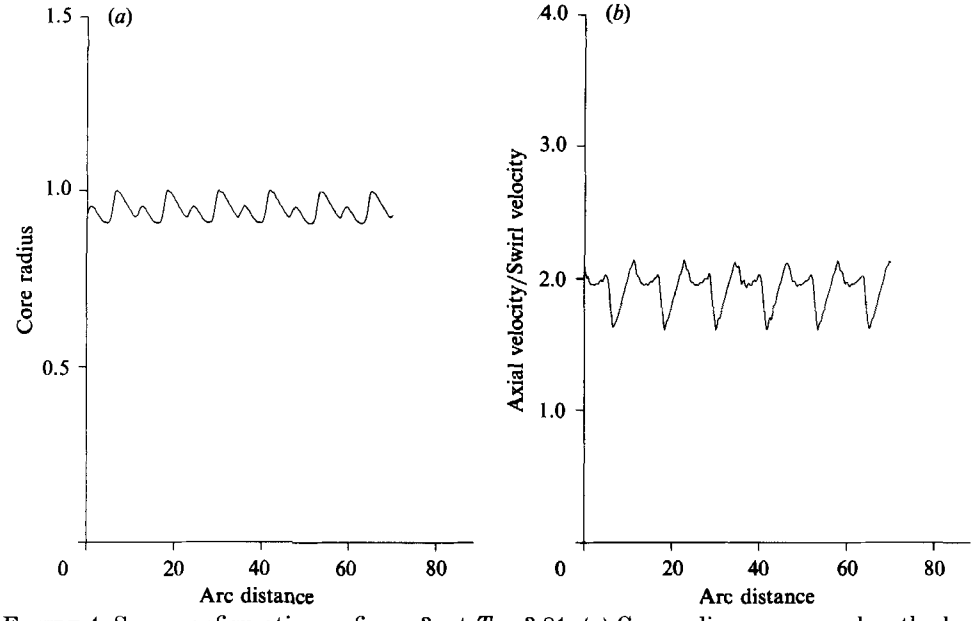

FIGURE 4. Same configuration as figure 3, at $T = 3.81$. (*a*) Core radius versus arc length along the ring. (*b*) Axial velocity divided by initial swirl velocity versus arc length.

time, with spatial derivatives approximated by left or right differences on alternate steps. This method was selected because of programming simplicity. The equations as written are in conservation form in the tangential direction. The Biot–Savart integral, (1.1) with $\mu^2 = 0.22\sigma^2$ corresponding to uniform vorticity in the core, was integrated using cubic splines to determine the tangent vectors. Nodes were inserted as required by a criterion based on local curvature and stretching (Ashurst & Meiburg 1988). Some computations were done using a large fixed number (of order 300) of nodes for comparison. All computations reported in this section were based

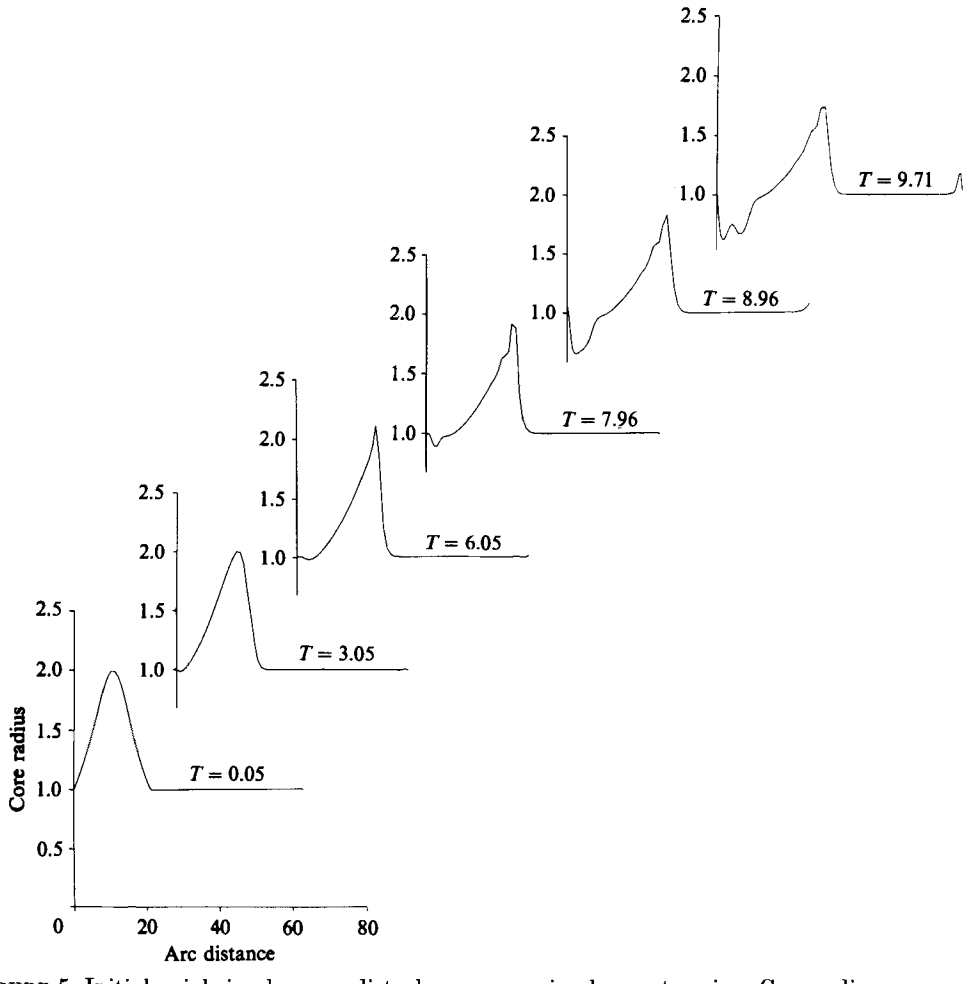

FIGURE 5. Initial axial simple wave disturbance on a circular vortex ring. Core radius versus arc length at several times showing steepening of the front and stretching at the rear.

on perturbations from an initially circular ring of radius $10\sigma_0$. The ring geometry was selected because of boundedness and periodicity.

The computations carried out were intended to test the growth of helical disturbances on vortices with axial flow since instability of the axial flow is believed to be the cause of the spiralling disturbances associated with vortex breakdown. The linearized theory of the stability of helical disturbances on a straight uniform vortex with axial slug flow of WB and Lessen *et al.* (1973), which was discussed in §3, shows instability of helical disturbances of wavenumber k if

$$(|w|/V_{\max})\, k\sigma_0 > \sqrt{2}-1, \tag{5.1}$$

where $V_{\max}$ is the maximum swirling velocity defined before. Since the jet without swirl is unstable for all wavenumbers, swirl has a stabilizing effect on long waves. When w is positive, right-handed helices with wavelength L will grow when

$$L/\sigma_0 < 15.2w/V_{\max}, \tag{5.2}$$

longer disturbances being stable.

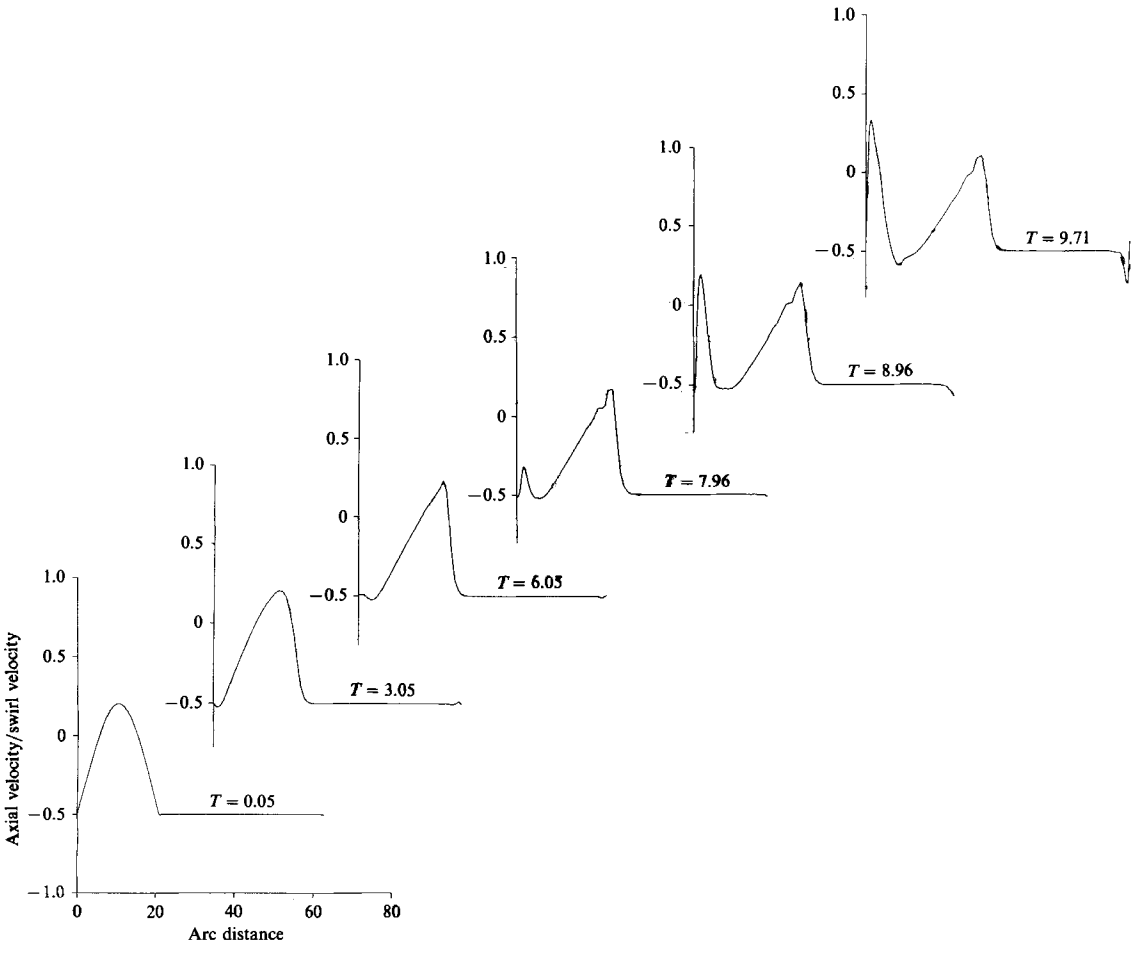

FIGURE 6. Initial simple wave disturbance on a circular vortex ring. Axial velocity divided by initial swirl velocity versus arc length showing decrease in axial velocity magnitude at the rear of the wave.

To test this in the ring geometry, the vortex ring was given an axial velocity equal to $2V_{\max}$ and was perturbed from its circular shape by displacing it from the plane with a sinusoidal displacement $x = 0.1\sigma_0 \sin(n\theta)$ and using 240 fixed nodes. For $n = 6$ the initial wavelength of $10.5\sigma_0$ is much shorter than the straight vortex critical value $30.4\sigma_0$. The results are shown in figure 3 where six helical waves rapidly grow to finite amplitude. The growth rate is comparable to predictions from the intrinsic equations, but the computation was stopped, because of inadequate resolution of the very twisted sections, before the maximum amplitude predicted by that analysis was reached, so we do not know if there is a tendency to oscillate in this geometry. Figures 4(*a*) and 4(*b*) show the vortex radius and the axial velocity at the last time shown in figure 3. These quantities are not quite constant around the ring but show growing periodic variation and the axial velocity in particular shows very rapidly varying shock-like behaviour.

A computation was done to test the spontaneous growth of a helix on an axial wave propagating into an approaching stream on the vortex ring. The maximum area ratio in the wave was taken as 4 and the velocity of the approach stream was

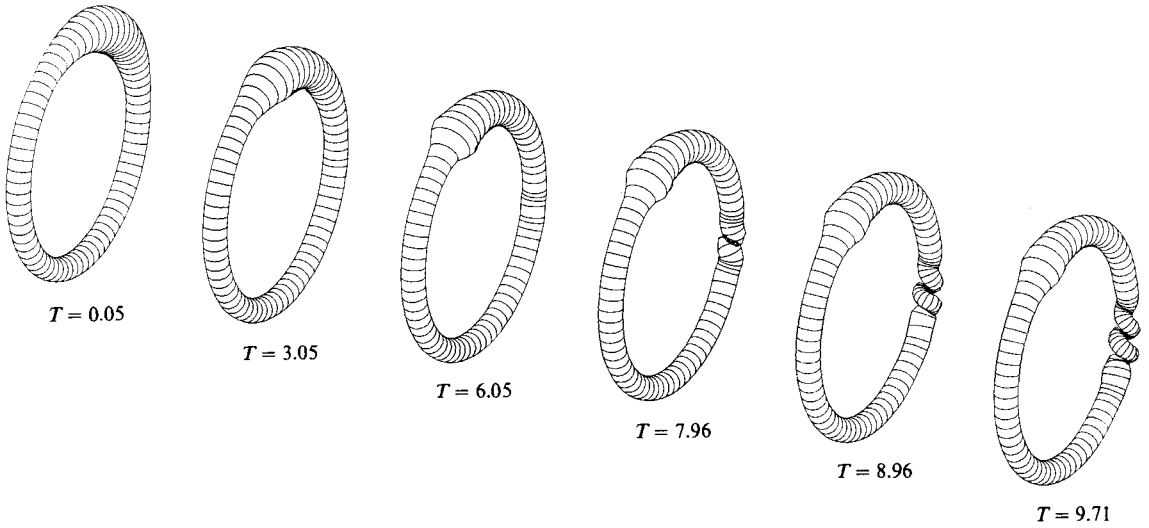

FIGURE 7. Initial simple wave disturbance on a circular vortex ring. Perspective views of the vortex ring showing steepening of the front with time and the growth of a helical wave at the rear in the region where figure 5 shows axial stretching. The viewpoint is from $x = 50\sigma_0$, $y = 86\sigma_0$, $z = 50\sigma_0$.

$w_1 = -0.5V_{1\max}$, these being realistic values for vortex breakdown from the Garg & Leibovich experiments (Leibovich 1978). The initial core radius distribution was taken to be

$$\left.\begin{aligned} \sigma &= \sigma_0[1-0.75(3\theta/\pi)(2-3\theta/\pi)]^{-\frac{1}{2}} \quad \text{on } 0 < \theta < \tfrac{2}{3}\pi \\ \sigma &= \sigma_0 \qquad\qquad\qquad\qquad\qquad\quad \text{on } \tfrac{2}{3}\pi < \theta < 2\pi, \end{aligned}\right\} \tag{5.3}$$

a parabolic distribution of λ on $\frac{1}{3}$ of the ring. The initial axial velocity was taken to be appropriate for a right travelling simple wave (on a straight vortex), with the Riemann invariant $w+2c$ equal to a constant. The initial condition is thus

$$w/V_{1\max} = -0.5+\sqrt{2}(1-\sigma_0/\sigma). \tag{5.4}$$

The maximum velocity in this profile is $0.21V_{1\max}$, in the opposite direction to the approach flow. (The maximum velocity is 0.42 times the local $V_{\max}$.) The results are shown in figures 5, 6 and 7. The core radius profile in figure 5 propagates forward, steepening on the front side. After about 8 time units a stretched out region begins to appear at the rear of the wave and becomes increasingly stretched out with time as can be seen from the reduced size of the core radius. The velocity in figure 6 shows a corresponding large decrease in magnitude in the same region. Both of these quantities are plotted versus arc length along the vortex core measured from a Lagrangian point which was initially at the tail of the wave. In figure 7 a series of perspective views of the vortex clearly show the steepening of the wave front and the growth of about 2 wavelengths of a helix in the stretched out region at the rear of the wave. The helix, initiated by the non-uniformity of the initial conditions, starts with one loop and continues to wind up new turns. The region with positive velocity near the middle and front of the wave is almost as unstable and would also grow a helical wave (of the opposite handedness) if one were excited. In fact this would be more like the disturbances seen in the vortex breakdown phenomenon. The individual waves of the helix can also be seen in the core radius plot. The wavelength

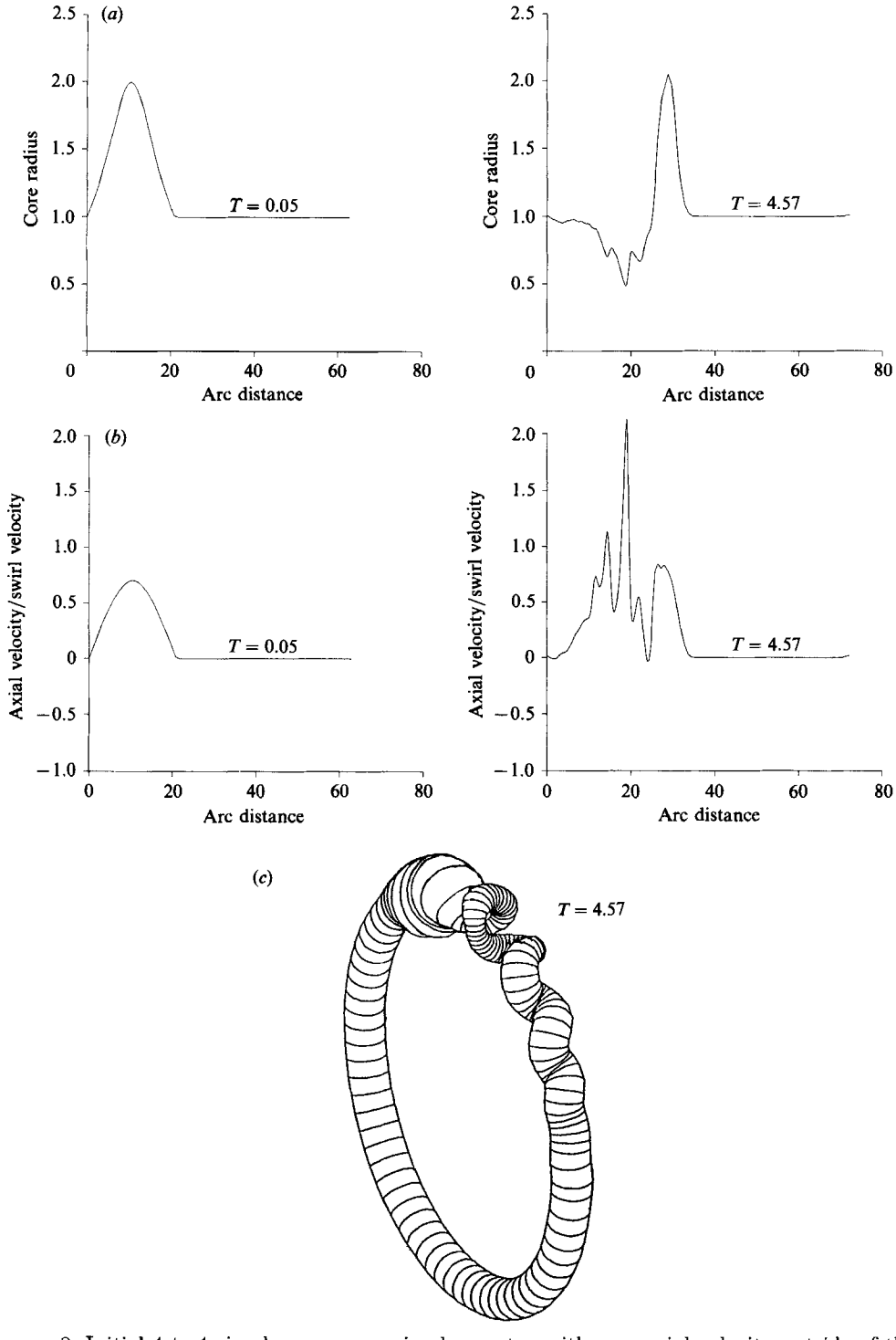

FIGURE 8. Initial 4 to 1 simple wave on a circular vortex with zero axial velocity outside of the simple wave. A small initial out of plane three-wave sinusoidal perturbation is given to the middle half of the simple wave. (*a*) Core radius versus arc length at two times. (*b*) Axial velocity divided by initial swirl velocity versus arc length at the same two times. (*c*) Perspective view of the vortex ring at the later time.

is obviously very short for these equations, about 4σ. Short waves of a similar nature are observed behind vortex breakdowns (Maxworthy, Hopfinger & Redekopp 1985).

There were 70 nodes at the beginning of the computation and this increased to 97 by the end. Since these were mostly added in the helix region, there were about 15 nodes to resolve each wavelength of the helix.

As a final example we have computed one more 4 to 1 simple wave with core variation given by (5.3), but with zero approach velocity so that the axial velocity is given by (5.4) without the '-0.5' term. Now the axial velocity is positive in the simple wave and a right-handed helix should grow. We have initiated a disturbance by placing an initial out of plane three wave sinusoidal disturbance with amplitude $0.05\sigma_0$ on the middle half of the simple wave. The results are shown in figure 8, where (*a*) and (*b*) show the core radius and axial velocity at the initial time and at one later time. Figure 8(*c*) shows a perspective view of the right-handed helix which emerges. This example simulates a vortex breakdown front, with trailing unstable transition to turbulence, propagating on a vortex which has no initial axial velocity, i.e. turbulence propagating into a stable region. While we know of no examples of strong vortex breakdown propagating on a vortex core with zero axial velocity, the result is similar to the breakdowns reported by Leibovich in which the upstream state has a stable Gaussian velocity profile and the vortex breakdown changes the parameters of the axial flow such that it becomes unstable to helical disturbances and finally becomes turbulent, i.e. it is propagating turbulence.

7. Discussion

The equations under study here have been derived subject to several limitations. First of all, the cross-section of the vortex tube is assumed to be approximately circular. This may not be the case when there is significant cross-flow. There could be a tendency for the vortex to fission into more than one core as observed for a jet in a cross-flow. Also, the derivation was for a vortex tube with radius of curvature much longer than the core radius. The short helical waves, which appear in figures 7 and 8, are marginal. We hope they are at least qualitatively represented. A danger is that real helical waves could be excited accidentally at the wavelength of the nodal separation, but this possibility has been suppressed by always keeping the nodal spacing much shorter than the wavelength of any short structures that appear.

This work was supported by the US Department of Energy, Office of Basic Energy Sciences, Division of Chemical Sciences. T.S.L. was a visitor to the Combustion Research Facility at Sandia National Laboratories under the Summer Faculty Program (1985).

Appendix A. Intrinsic equations for the motion of a vortex tube

Starting with the Frenet–Serret formulae

$$\partial\hat{\boldsymbol{t}}/\partial s = \kappa\hat{\boldsymbol{n}}, \quad \partial\hat{\boldsymbol{n}}/\partial s = -\kappa\hat{\boldsymbol{t}}+\tau\hat{\boldsymbol{b}}, \quad \partial\hat{\boldsymbol{b}}/\partial s = -\tau\hat{\boldsymbol{n}}, \tag{A 1}$$

and the local representation of the velocity fields which gives

$$\partial\boldsymbol{r}/\partial t = (W_{\mathrm{B}}+w)\,\hat{\boldsymbol{t}}+(U_{\mathrm{B}}+n)\,\hat{\boldsymbol{n}}+(V_{\mathrm{B}}+v)\,\hat{\boldsymbol{b}}, \tag{A 2}$$

differentiate the last equation with respect to ξ, using $\partial \boldsymbol{r}/\partial\xi = \lambda\hat{\boldsymbol{t}}$ and (A 1) to obtain

$$\frac{\partial\lambda}{\partial t}\hat{\boldsymbol{t}}+\lambda\frac{\partial\hat{\boldsymbol{t}}}{\partial t}=\frac{\partial(W_{\mathrm{B}}+w)}{\partial\xi}\hat{\boldsymbol{t}}+(W_{\mathrm{B}}+w)\lambda\kappa\hat{\boldsymbol{n}}+\frac{\partial(U_{\mathrm{B}}+u)}{\partial\xi}\hat{\boldsymbol{n}}+(U_{\mathrm{B}}+u)\lambda(\tau\hat{\boldsymbol{b}}-\kappa\hat{\boldsymbol{t}})$$
$$+\frac{\partial(V_{\mathrm{B}}+v)}{\partial\xi}\hat{\boldsymbol{b}}+(V_{\mathrm{B}}+v)\lambda\tau\hat{\boldsymbol{n}}. \quad \text{(A 3)}$$

Taking the $\hat{\boldsymbol{t}}$ component of this (using $\hat{\boldsymbol{t}}\cdot\partial\hat{\boldsymbol{t}}/\partial t = 0$) gives

$$\partial\lambda/\partial t = \partial(W_{\mathrm{B}}+w)/\partial\xi-(U_{\mathrm{B}}+u)\lambda\kappa, \quad \text{(A 4)}$$

and using this to eliminate $\partial\lambda/\partial t$ from (A 3) leaves

$$\partial\hat{\boldsymbol{t}}/\partial t = A_1\hat{\boldsymbol{n}}+A_2\hat{\boldsymbol{b}}, \quad \text{(A 5)}$$

where A_1 and A_2 are defined by (3.12) and (3.13). This process is repeated, differentiating (A 5) with respect to ξ to obtain

$$\frac{\partial(\lambda\kappa)}{\partial t}\hat{\boldsymbol{n}}+\lambda\kappa\frac{\partial\hat{\boldsymbol{n}}}{\partial t}=\frac{\partial A_1}{\partial\xi}\hat{\boldsymbol{n}}+A_1\lambda(\tau\hat{\boldsymbol{b}}-\kappa\hat{\boldsymbol{t}})+\frac{\partial A_2}{\partial\xi}\hat{\boldsymbol{b}}-A_2\lambda\tau\hat{\boldsymbol{n}}. \quad \text{(A 6)}$$

Take the scalar product with $\hat{\boldsymbol{n}}$ (using $\hat{\boldsymbol{n}}\cdot\partial\hat{\boldsymbol{n}}/\partial t = 0$) to obtain

$$\partial(\lambda\kappa)/\partial t = \partial A_1/\partial\xi - A_2\lambda\tau. \quad \text{(A 7)}$$

Using this to eliminate $\partial(\lambda\kappa)/\partial t$ from (A 6) gives

$$\partial\hat{\boldsymbol{n}}/\partial t = B_1\hat{\boldsymbol{b}}-A_1\hat{\boldsymbol{t}}. \quad \text{(A 8)}$$

Repeat this process again by differentiating (A 8) with respect to ξ to find

$$\partial(\lambda\tau)/\partial t = \lambda\kappa A_2+\partial B_1/\partial\xi, \quad \text{(A 9)}$$

and

$$\partial\hat{\boldsymbol{b}}/\partial t = -A_2\hat{\boldsymbol{t}}-B_1\hat{\boldsymbol{n}}. \quad \text{(A 10)}$$

The final step is to write (2.11) in the form

$$\frac{\partial w}{\partial t}\hat{\boldsymbol{t}}+w\frac{\partial\hat{\boldsymbol{t}}}{\partial t}+2\frac{\partial u}{\partial t}\hat{\boldsymbol{n}}+2u\frac{\partial\hat{\boldsymbol{n}}}{\partial t}+2\frac{\partial v}{\partial t}\hat{\boldsymbol{b}}+2v\frac{\partial\hat{\boldsymbol{b}}}{\partial t}=\left(\frac{w}{\lambda}\right)\frac{\partial(u\hat{\boldsymbol{n}}+v\hat{\boldsymbol{b}}-W_{\mathrm{B}}\hat{\boldsymbol{t}}-U_{\mathrm{B}}\hat{\boldsymbol{n}}-V_{\mathrm{B}}\hat{\boldsymbol{b}})}{\partial\xi}$$
$$+\left(\frac{\Gamma\lambda}{A_0}\right)\hat{\boldsymbol{t}}\times(w\hat{\boldsymbol{t}}+u\hat{\boldsymbol{n}}+v\hat{\boldsymbol{b}})+(\Gamma^2/8\pi A_0)\frac{\partial\ln(\lambda)}{\partial\xi}\hat{\boldsymbol{t}} \quad \text{(A 11)}$$

and substitute for $\partial\hat{\boldsymbol{t}}/\partial t$, $\partial\hat{\boldsymbol{n}}/\partial t$ and $\partial\hat{\boldsymbol{b}}/\partial t$ from (A 5), (A 8) and (A 10). The components of this equation are (3.9), (3.10) and (3.11), and (A 4), (A 7) and (A 9) are (3.6), (3.7) and (3.8).

Appendix B. Example of Benjamin's theory of vortex breakdown

A circular vortex tube is oriented along the z-axis. The flow is assumed to be frictionless and steady. The upstream state from which waves are supposed to arise has axial velocity W and swirl velocity V which are prescribed functions of $y(=\frac{1}{2}r^2)$. The stream function $\Psi_{\mathrm{A}}(y)$ for the primary flow is defined by $W = \mathrm{d}\Psi_{\mathrm{A}}/\mathrm{d}y$, $\Psi_{\mathrm{A}}(0) = 0$, and the pressure can be found by integrating $\mathrm{d}p/\mathrm{d}y = \rho V^2/2y$. Hence the Bernoulli constant $H = p/\rho+\frac{1}{2}(W^2+V^2)$ and the quantity $I = yV^2$, which is

proportional to the square of the circulation, can be expressed as functions of y or Ψ_A.

In a state of motion arising from the primary state H and I keep their original values along stream surfaces. Benjamin (1962) showed that these properties require the stream function to satisfy

$$\frac{\partial^2\Psi}{\partial y^2}+\frac{1}{2y}\frac{\partial^2\Psi}{\partial z^2}=H'(\Psi)+\frac{I'(\Psi)}{2y}, \tag{B 1}$$

where $H(\Psi)$ and $I(\Psi)$ have the same forms as the functions $H(\Psi_A)$ and $I(\Psi_A)$ derived for the primary flow. The boundary conditions are $\Psi(z,0)=0$ and $\partial\Psi(z,\infty)/\partial y=\partial\Psi_A(z,\infty)/\partial y$.

A uniform solution $\Psi=\Psi_B(y)\neq\Psi_A(y)$ of the ordinary differential equation

$$\frac{\mathrm{d}^2\Psi}{\mathrm{d}y^2}=H'(\Psi)+\frac{I'(\Psi)}{2y}, \tag{B 2}$$

is said to be conjugate to the primary solution $\Psi_A(y)$. This is to be thought of as the uniform state downstream of the vortex breakdown. Equation (B 1) describes the transition between the two uniform conjugate states.

As an example consider the case where the primary state is a hollow vortex of radius σ_A with slug flow in the core,

$$\left.\begin{aligned} W&=W_0 \quad (r>\sigma_A)\\ &=W_A \quad (r<\sigma_A),\end{aligned}\right\} \tag{B 3}$$

and

$$\left.\begin{aligned} V&=\Gamma/2\pi r \quad (r>\sigma_A)\\ &=0 \qquad\quad (r<\sigma_A),\end{aligned}\right\} \tag{B 4}$$

where $(-W_0)$ is the constant speed of propagation of the wave if it were seen in a non-stationary frame.

The functions $H(\Psi)$ and $I(\Psi)$ are found to be

$$\left.\begin{aligned} H&=\tfrac{1}{2}W_0^2 \qquad\qquad\qquad (\Psi>\tfrac{1}{2}W_A\sigma_A^2)\\ &=-\frac{\Gamma^2}{8\pi^2\sigma_A^2}+\tfrac{1}{2}W_A^2 \quad (\Psi<\tfrac{1}{2}W_A\sigma_A^2),\end{aligned}\right\} \tag{B 5}$$

and

$$\left.\begin{aligned} I&=\Gamma^2/8\pi^2 \quad (\Psi>\tfrac{1}{2}W_A\sigma_A^2)\\ &=0 \qquad\quad\;\; (\Psi<\tfrac{1}{2}W_A\sigma_A^2).\end{aligned}\right\} \tag{B 6}$$

Since H and I are constant in both the inner and outer regions it follows that $\mathrm{d}^2\Psi/\mathrm{d}y^2=0$ in each of these regions, therefore in the downstream conjugate state W is constant on each side of a discontinuity at $r=\sigma_B$. Conservation of mass and the boundary condition at infinity give

$$\left.\begin{aligned} W&=W_0 \qquad\qquad\quad (r>\sigma_B)\\ &=W_B<W_A\sigma_A^2/\sigma_B^2 \quad (r<\sigma_B).\end{aligned}\right\} \tag{B 7}$$

Then (A 6) and the definition of I give

$$\left.\begin{aligned} V&=\Gamma/2\pi r \quad (r>\sigma_B)\\ &=0 \qquad\quad (r<\sigma_B).\end{aligned}\right\} \tag{B 8}$$

Therefore the conjugate state is a hollow vortex of radius σ_B with slug flow in its core. These could be called self-similar or co-conjugate states.

There is more information to be obtained here. Since the pressure across the interface at $r = \sigma_B$ must be continuous, and H, V and W are discontinuous, the definition of H requires continuity of $H - \frac{1}{2}(W^2 + V^2)$. Thus

$$-\frac{\Gamma^2}{8\pi^2\sigma_B^2} = -\frac{\Gamma^2}{8\pi^2\sigma_A^2} - \tfrac{1}{2}W_B^2 + \tfrac{1}{2}W_A^2. \tag{B 9}$$

This equation and

$$W_A \sigma_A^2 = W_B \sigma_B^2 \tag{B 10}$$

may be solved for

$$W_A = \pm V_{A\max}/(1 + \sigma_A^2/\sigma_B^2)^{\frac{1}{2}}, \tag{B 11}$$

where $V_{A\max} = \Gamma/2\pi\sigma_A$. To put this in a form to be compared with (3.12) and (3.13) in which a wave is propagating to the right, identify state A with state 1 and state B with state 2 and subtract W_0 from all velocities, defining $w_1 = W_A - W_0$, $w_2 = W_B - W_0$ and denote by W the propagation speed $(-W_0)$. Then

$$W = w_1 + V_{1\max}/(1 + A_1/A_2)^{\frac{1}{2}} \tag{B 12}$$

is the same as (4.14), and

$$w_2 - w_1 = W_B - W_A = W_A(A_1/A_2 - 1) \tag{B 13}$$

gives (4.15). This appears to be the only example of Benjamin's theory for which jump conditions have been formulated.

REFERENCES

Ashurst, W. T. & Meiburg, E. 1988 Three-dimensional shear layers via vortex dynamics. *J. Fluid Mech.* **189**, 87–116.

Benjamin, T. B. 1962 Theory of the vortex breakdown phenomenon. *J. Fluid Mech.* **14**, 593–629.

Benjamin, T. B. 1967 Some developments in the theory of vortex breakdown. *J. Fluid Mech.* **28**, 65–84.

Betchov, R. 1965 On the curvature and torsion of an isolated vortex filament. *J. Fluid Mech.* **22**, 471–479.

Escudier, M. P., Bornstein, J. & Maxworthy, T. 1982 The dynamics of confined vortices. *Proc. R. Soc. Lond.* A **382**, 335–360.

Faler, J. H. & Leibovich, S. 1978 An experimental map of the internal structure of a vortex breakdown. *J. Fluid Mech.* **86**, 313–335.

Garg, A. K. & Leibovich, S. 1979 Spectral characteristics of vortex breakdown flow fields. *Phys. Fluids* **22**, 2053–2070.

Kelvin, Lord 1880 Vibrations of a columnar vortex. *Phil. Mag.* **10**, 155–168.

Lamb, H. 1932 *Hydrodynamics*, §187. Dover.

Leibovich, S. 1978 The structure of vortex breakdown. *Ann. Rev. Fluid Mech.* **10**, 221–246.

Leonard, A. 1985 Computing three-dimensional incompressible flows with vortex elements. *Ann. Rev. Fluid Mech.* **17**, 523–559.

Lessen, M., Deshpande, N. V. & Hadji-Ohanes, B. 1973 Stability of a potential vortex with a non-rotating and rigid-body rotating top-hat jet core. *J. Fluid Mech.* **60**, 459–456.

Lessen, M., Singh, P. J. & Paillet, F. 1974 The stability of a trailing line vortex. Part 1. Inviscid theory. *J. Fluid Mech.* **63**, 753–763.

MacCormack, R. 1971 Numerical solution of the interaction of a shock wave with a laminar boundary layer. In *Proc. of the Second Intl Conf. on Numerical Methods in Fluid Mech.* (ed. M. Holt). Lecture Notes in Physics, vol. 8, pp. 151–163. Springer.

Maxwothy, T., Hopfinger, E. J. & Redekopp, L. G. 1985 Wave motions on vortex cores. *J. Fluid Mech.* **151**, 141–165.

Maxwothy, T., Mory, M. & Hopfinger, E. J. 1983 Waves on vortex cores and their relation to vortex breakdown. In *Proc. AGARD Conf. on Aerodynamics of Vortical Type Flows in Three Dimensions*; *CPP*-342, paper 29.

Moore, D. W. 1972 Finite amplitude waves on aircraft trailing vortices. *Aero. Q.* **23**, 307–314.

Moore, D. W. & Saffman, P. G. 1972 The motion of a vortex filament with axial flow. *Phil. Trans. R. Soc. Lond.* A **272**, 407–429.

Moore, D. W. & Saffman, P. G. 1975 The instability of a straight vortex filament in a strain field. *Proc. R. Soc. Lond.* A **346**, 413–425.

Rosenhead, L. 1930 The spread of vorticity in the wake behind a cylinder. *Proc. R. Soc. Lond.* A **127**, 590.

Sarpkaya, T. 1971 On stationary and travelling vortex breakdown. *J. Fluid Mech.* **45**, 545–559.

Van Leer, B. 1979 Towards the ultimate conservative difference scheme. V. A second order sequel to Godunov's method. *J. Comp. Phys.* **32**, 101–136.

Widnall, S. & Bliss, D. 1971 Slender-body analysis of the motion and stability of a vortex filament containing an axial flow. *J. Fluid Mech.* **50**, 335–353.

Widnall, S., Bliss, D. & Tsai, C.-Y. 1974 The instability of short waves on a vortex ring. *J. Fluid Mech.* **60**, 35–47.

Widnall, S., Bliss, D. & Zalay, A. 1971 Theoretical and experimental study of the stability of a vortex pair. In *Aircraft Wake Turbulence and its Detection*, pp. 305–338. Plenum.

Whitham, G. B. 1974 *Linear and Nonlinear Waves*, chap. 13. Wiley.